

# Jitter radiation as a possible mechanism for Gamma-Ray Burst afterglows. Spectra and lightcurves

Mikhail V. Medvedev<sup>1</sup>,

*Department of Physics and Astronomy, University of Kansas, KS 66045*

Davide Lazzati, Brian C. Morsony and Jared C. Workman

*JILA, University of Colorado, 440 UCB, Boulder, CO 80309-0440*

## ABSTRACT

The standard model of GRB afterglows assumes that the radiation observed as a delayed emission is of synchrotron origin, which requires the shock magnetic field to be relatively homogeneous on small scales. An alternative mechanism – jitter radiation, which traditionally has been applied to the prompt emission – substitutes synchrotron when the magnetic field is tangled on a microscopic scale. Such fields are produced at relativistic shocks by the Weibel instability. Here we explore the possibility that small-scale fields populate afterglow shocks. We derive the spectrum of jitter radiation under the afterglow conditions. We also derive the afterglow lightcurves for the ISM and Wind profiles of the ambient density. Jitter self-absorption is calculated here for the first time. We find that jitter radiation can produce afterglows similar to synchrotron-generated ones, but with some important differences. We compare the predictions of the two emission mechanisms. By fitting observational data to the synchrotron and jitter afterglow lightcurves, it can be possible to discriminate between the small-scale vs large-scale magnetic field models in afterglow shocks.

*Subject headings:* gamma rays: bursts — radiation processes — shock waves — magnetic fields

## 1. Introduction

The general framework for the interpretation of the long-wavelength radiation of gamma-ray burst (GRB) afterglows is the external shock synchrotron model (Meszaros & Rees 1997;

---

<sup>1</sup> Also at the Institute for Nuclear Fusion, RRC “Kurchatov Institute”, Moscow 123182, Russia

Waxman 1997; Piran 1999). In that scenario, a blastwave is generated by the interaction of the GRB ejecta with the interstellar medium. At the shock front, electrons are accelerated in a power-law distribution with energy (or with Lorentz factor  $\gamma$ ) and a strong magnetic field is generated by some mechanism. The model assumes that the magnetic field is coherent on the Larmor scale of the emitting electron, hence allowing for synchrotron emission. Both the relativistic electron population and the magnetic field are originally thought to share a sizable fraction of  $\sim 10\%$  of the internal energy of the blastwave; those fractions are being called  $\epsilon_e$  and  $\epsilon_B$ , respectively. Afterglow spectral fits yield typical values,  $\epsilon_e \sim 0.1 - 0.01$  and  $\epsilon_B \sim 0.01 - 0.0001$ , with relatively large scatter (Panaiteescu & Kumar 2001; Panaiteescu 2006).

No mechanism or instability capable of generating a sub-equipartition magnetic field in GRBs has been identified for a while, until Medvedev & Loeb (1999) suggested that the field can be generated through the Weibel instability. This prediction has been extended to non-relativistic shocks, e.g., in supernovae and galaxy clusters (Medvedev, Silva, Kamionkowski 2006), and confirmed via numerical PIC simulations (Silva, et al. 2003; Nishiwawa, et al. 2003; Frederiksen et al. 2004; Medvedev, et al. 2005; Spitkovski 2005). The volume-averaged value of  $\epsilon_B$  deduced from the simulation is indeed  $\sim 0.01 - 0.0001$  (depending on location with respect to the main shock compression). An intriguing relation:

$$\epsilon_e \simeq \epsilon_B^{1/2}, \quad (1)$$

recently found by Medvedev (2006b), can allow one to reduce the number of fit parameters in afterglow studies.

Weibel-generated fields have a very short coherence length-scale (smaller than  $1/\gamma^2$  times the electron Larmor radius) and standard synchrotron equations cannot be adopted. The theory of jitter radiation has been proposed by Medvedev (2000) and further developed in subsequent works (Medvedev 2006a; Fleishman 2006). (Note, however, that Fleishman 2006 incorrectly predicts the absence of steep spectral slopes, such as  $F_\nu \propto \nu^1$ , just below  $E_{\text{peak}}$  in GRBs).

Unlike synchrotron, jitter radiation is sensitive to the statistical properties of the magnetic field in the shock, that is to the spectrum of magnetic fluctuations, and not just to its “global property” – the strength (Medvedev 2000). In addition, the spectrum of jitter radiation depends on the shock viewing angle, i.e., the angle,  $\theta'$  between the shock velocity (= propagation direction) and the line of sight ( $\theta'$  is measured in the shock comoving frame). The two extreme cases are characterized by the emissivity function being a power-law at frequencies below the spectral peak:

$$P(\omega) \propto \omega^\alpha, \quad (2)$$

with  $\alpha = 1$  for  $\theta' = 0$  – a shock viewed face-on (this is also the case of the “effective” 1D magnetic turbulence, considered in Medvedev 2000), and  $\alpha = 0$  for  $\theta' = \pi/2$  – an edge-on shock (this is also the case in isotropic 2D and 3D turbulence). These asymptotes, along with a general case of  $0 \leq \theta' \leq \pi/2$ , are considered elsewhere (Medvedev 2006, Workman et al. in preparation). For reference, synchrotron radiation has  $\alpha = 1/3$  at low energies.

Should afterglows be resolved, one would observe a limb-brightened object (Granot et al. 1999). For a spherical outflow, the emission spectrum will be entirely dominated by the limb emission. Because of relativistic aberration, the photons emitted within an angle of  $\sim 1/\Gamma_{\text{sh}}$  with respect to the line of sight in the lab (observer’s) frame, have been emitted at angle  $\theta'$  in the shock comoving frame:

$$\cos \theta' = \frac{\cos(1/\Gamma_{\text{sh}}) - \beta_{\text{sh}}}{1 - \beta_{\text{sh}} \cos(1/\Gamma_{\text{sh}})} = 0, \quad (3)$$

where  $\beta_{\text{sh}}$  is the dimensionless shock speed. That is, these photons are emitted at the angle  $\theta' = 90^\circ$  away from the shock normal. This consideration is also true for a jet outflow at times when the jet opening angle is larger than  $1/\Gamma_{\text{sh}}$ .

In general, after the jet break, the emission will still be dominated by the limb. However, the shock there will not be seen edge-on, but rather at some angle  $\theta' < 90^\circ$ . The jitter spectrum is, in general, anisotropic, i.e., it depends on  $\theta'$ . There is a break,  $\nu_b(\theta')$  in the jitter spectrum (Medvedev 2006a) below the jitter peak,  $\nu_b < \nu_{\text{jitter peak}}$ , such that  $\alpha = 1$  above the break (at  $\nu_b < \nu < \nu_{\text{jitter peak}}$ ) and  $\alpha = 0$  below it (at  $\nu < \nu_b$ ). The dependence of the break frequency on  $\theta'$  is not easy to parameterize. Since the break is quite smooth is also not easy to establish its precise position. One characteristic point is:  $\nu_b \sim 0.01\nu_{\text{jitter peak}}$  at  $\theta' = \pi/10 = 18$  degrees.

Thus, for spherical outflows and for jets seen before the “jet break”, the reasonable approximation will be the “edge-on” shock, with  $\alpha = 0$ . However, at late times, especially when the jet becomes weakly relativistic, the “face-on” case with  $\alpha = 1$  should be a better approximation.

One cautious remark. The above consideration assumes strong anisotropy of the magnetic turbulence in the shock (Medvedev & Loeb 1999), which is likely true in the internal shocks. We do not understand well the properties of magnetic turbulence far downstream the external shock. If the magnetic turbulence will become nearly isotropic, then a 3D jitter regime gives  $\alpha = 0$ , independent of the viewing angle.

Below, we consider both the  $\alpha = 0$  and the  $\alpha = 1$  cases in calculating the jitter self-absorption frequency. This paper is organized as follows: in § 2 we summarize the shock kinematics, in § 3 we derive the jitter self absorption frequency in various regimes while in

§ 4 we compute all the observable properties of the spectrum. We summarize and discuss our results in § 5.

## 2. Shock kinematics

Here we summarize, for future use, the kinematic relations of several blast wave parameters. For a highly relativistic blast wave with Lorentz factor  $\Gamma_{\text{sh}}$ , the density jump condition relates the pre-shock ISM density to the density downstream,  $n'$ , measured in the shock frame:

$$n' \simeq 4\Gamma_{\text{sh}}n_{\text{ISM}}. \quad (4)$$

The magnetic field strength downstream

$$B' = (32\pi\Gamma_{\text{sh}}^2 n_{\text{ISM}} m_p c^2 \epsilon_B)^{1/2}, \quad (5)$$

where  $\epsilon_B$  is the magnetic field equipartition parameter. The minimum Lorentz factor of the accelerated electrons, which share a fraction  $\epsilon_e < 1$  of the total energy of the shock (outflow) is:

$$\gamma_m = \left( \frac{s-2}{s-1} \right) \frac{m_p}{m_e} \epsilon_e \Gamma_{\text{sh}} \approx 6.12 \times 10^2 \epsilon_e \Gamma_{\text{sh}}. \quad (6)$$

Here the last expression is calculated for a typical electron power-law index  $s = 2.5$ , see definition below, Eq (12).

### 2.1. Constant density ISM

The radius and Lorentz factor of a blast wave propagating in a constant density ISM depend on the observed time as (Granot et al. 1999)

$$\Gamma_{\text{sh}} \approx 3.65 \left( \frac{E_{52}}{n_{\text{ISM},0}} \right)^{1/8} \left( \frac{t_{\text{days}}}{1+z} \right)^{-3/8}, \quad (7)$$

$$R \approx 5.53 \times 10^{17} \left[ \frac{E_{52} t_{\text{days}}}{n_{\text{ISM},0} (1+z)} \right]^{1/4} \text{cm}. \quad (8)$$

Here  $E_{52} = E_{\text{explosion}}/10^{52}$  erg, and  $n_{\text{ISM},0} = n_{\text{ISM}}/1 \text{ cm}^{-3}$ .

### 2.2. Wind model

If the blast wave is propagating in the wind environment with the density decreasing with distance,  $n \propto r^{-2}$ , the Lorentz factor and the radius of the blast wave are (Chevalier & Li

2000)

$$\Gamma_{\text{sh}} \approx 4.96 E_{52}^{1/2} \left( \frac{A_* t_{\text{days}}}{1+z} \right)^{-1/4}, \quad (9)$$

$$R \approx 1.56 \times 10^{17} \left[ \frac{E_{52} t_{\text{days}}}{A_*(1+z)} \right]^{1/2} \text{ cm}. \quad (10)$$

Here the wind parameter  $A_* = [\dot{M}_w/(10^{-5} M_\odot \text{ yr}^{-1})]/[V_w/(10^3 \text{ km s}^{-1})]$ , where  $\dot{M}_w$  is the mass loss rate,  $V_w$  is the wind velocity. Since the ambient density is no longer constant, one need to substitute  $n_{\text{ISM}}$  with the wind density

$$n_{\text{wind}} = AR^{-2} \approx (3.00 \times 10^{35} A_* \text{ cm}^{-1}) R^{-2}. \quad (11)$$

### 3. Theory

Here we work in the shock comoving frame. Thus, all the frequencies are expressed in this frame. Also, all the shock parameters, such as the particle number density  $n'$  and magnetic field  $B'$ , are those in the shocked region and are measured in the comoving frame as well, unless stated otherwise. We use “prime” to denote quantities measured in the shock frame. Sometimes we omit “prime” when this does not cause any confusion.

We introduce the accelerated electron distribution function:

$$N(\gamma) = (s-1)N_e \gamma_m^{s-1} \gamma^{-s}, \quad \gamma \geq \gamma_m, \quad (12)$$

where  $s$  is the power-law index,  $\gamma_m$  is the minimum Lorenz factor (low-energy cut-off),  $N_e = 4\pi R^2 \Delta' n_{\text{ISM}}$  is the total number of the nonthermal (emitting) electrons,  $R$  is the radius of the blast wave,  $\Delta'$  is its thickness,  $n_{\text{ISM}}$  is the number density of the electrons in the ambient medium.

The absorption coefficient at comoving frequency  $\nu'$  is (Dermer et al. 2000):

$$\kappa_{\nu'} = \frac{1}{8\pi m_e V_{\text{bw}} \nu'^2} \int_1^\infty d\gamma P(\nu', \gamma) \gamma^2 \frac{\partial}{\partial \gamma} \left[ \frac{N(\gamma)}{\gamma^2} \right], \quad (13)$$

where  $V_{\text{bw}} = 4\pi r^2 \Delta'$  is the volume of the blast wave of the comoving thickness  $\Delta'$  and  $P(\nu', \gamma)$  is the emissivity function. Straightforwardly,

$$\gamma^2 \frac{\partial}{\partial \gamma} \left[ \frac{N(\gamma)}{\gamma^2} \right] = -(s+2)(s-1)N_e \gamma_m^{s-1} \gamma^{-s-1}. \quad (14)$$

### 3.1. Emissivity functions

We first discuss synchrotron, for reference. The synchrotron comoving peak frequency is at

$$\nu'_s = (3/2)\nu_B\gamma^2, \quad (15)$$

where  $\nu_B = eB'/2\pi m_e c$  is the cyclotron (Larmor) frequency in a homogeneous magnetic field of strength  $B'$ , the pitch-angle is assumed to be  $\pi/2$ , for simplicity. At  $\nu' \ll \nu'_s$ , the synchrotron emissivity is

$$P_{\text{synch}}(\nu', \gamma) \simeq \frac{e^2}{c} \sqrt{3} \nu_B \left[ \frac{4\pi}{\sqrt{3}\Gamma(1/3)} \left( \frac{\nu'}{3\nu_B\gamma^2} \right) \right], \quad (16)$$

where  $\Gamma(1/3) \simeq 2.68$  is a gamma function.

The jitter peak frequency is determined by the magnetic field spectrum in the post-shock medium. Recent numerical simulations (Frederiksen et al. 2004; Medvedev, Silva, Kamionkowski 2006) demonstrate that the field generation by both the electrons and the protons, occurs well before the main shock compression. The wave-vector of the fastest growing mode of the Weibel instability in the linear regime is (Medvedev & Loeb 1999):

$$k_{\text{Weibel}} \approx 2^{-1/4}(\omega_{p,e}/c)\bar{\gamma}_e^{-1/2}, \quad (17)$$

where  $\omega_{p,e} = \sqrt{4\pi e^2 n/m_e} \approx 5.64 \times 10^4 n^{1/2} \text{ s}^{-1}$  is the plasma frequency. Because  $\omega_{p,e}$  is a Lorentz invariant,  $k_{\text{Weibel}}$  is determined by the parameters of the ambient, unshocked medium alone. Thus, the density  $n = n_{\text{ISM}}$  is the ambient medium density, and the mean Lorentz factor of the electrons in the ambient medium,  $\bar{\gamma}_e$ , is close unity (the ISM is cold, non-relativistic). The shock compression and the proton thermalization occur far downstream, significantly behind the region where the field has been generated. Therefore, the correlation length of the field decreases (primarily in the parallel direction) because of the compression. Hence, the characteristic wave-vector of the downstream random fields is

$$k_{\text{rand}} \simeq (4\Gamma_{\text{sh}})k_{\text{Weibel}}. \quad (18)$$

Numerical simulations also indicate that the correlation scale of the field  $\lambda_B = 2\pi/k_{\text{rand}}$  varies with distance from the shock front because of the highly nonlinear dynamics of the Weibel-generated currents and fields (Frederiksen et al. 2004; Medvedev, et al. 2005). We therefore parameterize this as

$$k_{\text{rand}} = \eta(\omega_{p,e}/c), \quad (19)$$

where the parameter  $\eta$  incorporates all relativistic effects, the shock compression and the nonlinear evolution of the Weibel turbulence. Thereafter, we use

$$\eta \simeq 2^{-1/4}(4\Gamma_{\text{sh}})\bar{\gamma}_e^{-1/2} \simeq 2^{7/4}\Gamma_{\text{sh}}, \quad (20)$$

where we assumed that  $\bar{\gamma}_e \sim 1$ .

The characteristic frequency of the electron's jitter while it moves at roughly the speed of light through these magnetic fields is  $\nu \sim c/\lambda_B$ . More precisely,

$$\nu_r = k_{\text{rand}} c / 2\pi = \eta \omega_{p,e} / 2\pi = \eta \nu_{p,\text{ISM}}, \quad (21)$$

where we introduced the plasma frequency of the ISM,  $\nu_{p,\text{ISM}} = (4\pi e^2 n_{\text{ISM}} / m_e)^{1/2} / 2\pi = 8.98 \times 10^3 n_{\text{ISM}}^{1/2} \text{ Hz}$ .

The peak of the emitted jitter radiation is  $\nu'_j \sim \nu_r \gamma^2$ , but its exact position slightly depends on the magnetic field spectrum, defined as  $(B'^2)_k \propto k^{2\mu}$ . For steep spectra,  $\mu \gg 1$ , the peak is at, roughly, twice the jitter frequency:

$$\nu'_j \simeq 2\nu_r \gamma^2. \quad (22)$$

The jitter and synchrotron peak frequencies in the magnetic fields of identical strengths are related to each other via the identities

$$\nu_r = \nu_B / \delta, \text{ or } \nu'_j = \nu'_s / (3\delta/4), \quad (23)$$

These identities define the parameter  $\delta \lesssim 1$ , which is the ratio of the deflection angle of the particle path in chaotic fields to the beaming angle  $1/\gamma$  (Medvedev 2000). It is expressed via the magnetic field equipartition parameter in the shock,  $\epsilon_B$ , as

$$\delta = \left( \frac{m_p}{m_e} \frac{8\Gamma_{\text{sh}}}{\eta^2} \epsilon_B \right)^{1/2} \simeq \left( \frac{m_p}{m_e} 2^{-1/2} \epsilon_B \right)^{1/2} \approx 36.0 \sqrt{\epsilon_B}. \quad (24)$$

The jitter emissivity function below the peak is

$$P_{\text{jitter}}(\nu', \gamma) \simeq \frac{e^2}{c} \pi f(\mu) \delta^2 \nu_r \left( \frac{\nu'}{2\nu_r \gamma^2} \right)^\alpha. \quad (25)$$

Later on, we neglected a factor  $f(\mu) = (2\mu + 1)/(2\mu - 1)$  (calculated for  $\alpha = 1$ ) because it is of order unity when  $\mu \gg 1$ .

Thus, for both emission mechanisms,

$$P(\nu', \gamma) \simeq a \left( \frac{\nu'}{b\gamma^2} \right)^\alpha. \quad (26)$$

Here, for synchrotron

$$a = \frac{e^2}{c} \frac{4\pi}{\Gamma(1/3)} \nu_B, \quad b = 3\nu_B, \quad \alpha = 1/3, \quad (27)$$

and for jitter

$$a = \frac{e^2}{2c} \pi \delta^2 \nu_r, \quad b = \nu_r, \quad \alpha = 0, \text{ and } \alpha = 1. \quad (28)$$

### 3.2. Self-absorption frequencies for $\nu_a < \nu_m$

Here we assume that the self-absorption frequency is below the jitter peak in the spectrum from the ensemble of the electrons,  $\nu'_a \lesssim \nu'_m = 2\nu_{j,m} \equiv 2\nu_r \gamma_m^2$ .

The opacity is easily calculated from Eqs. (14), (26) to yield

$$\kappa_{\nu'} = \frac{(s+2)(s-1)N_e a b^{-\alpha} (\nu')^{\alpha-2}}{8\pi m_e V_{\text{bw}}(s+2\alpha)\gamma_m^{2\alpha+1}}. \quad (29)$$

The self-absorption frequency is that, at which the optical thickness of the blast wave shell is unity:

$$\kappa_{\nu'_a} \Delta' \sim 1. \quad (30)$$

This condition gives:

$$\nu_a'^{2-\alpha} \simeq \frac{(s+2)(s-1)}{(s+2\alpha)} \frac{R n_{\text{ISM}} a b^{-\alpha}}{24\pi m_e \gamma_m^{2\alpha+1}}. \quad (31)$$

This equation works for both synchrotron and jitter radiation. One just need to replace the general parameters  $a, b, \alpha$  with those above, for a process of interest.

For jitter radiation, we have

$$a b^{-\alpha} = \frac{e^2}{c} \frac{\pi}{2^\alpha} \delta^2 \nu_r^{1-\alpha}. \quad (32)$$

Therefore,

$$\nu_a'^{2-\alpha} \simeq \frac{(s+2)(s-1)}{(s+2\alpha)} \frac{\pi}{24} \frac{(R/c)\nu_{p,\text{ISM}}^2 \nu_r^{1-\alpha} \delta^2}{\gamma_m^{2\alpha+1}}. \quad (33)$$

#### 3.2.1. Case $\alpha = 0$

In this case,

$$\begin{aligned} \nu'_a &\simeq \left( \frac{\pi}{24} \frac{(s+2)(s-1)}{s} \right)^{1/2} \frac{(R/c)^{1/2} \nu_{p,\text{ISM}} \nu_r^{1/2} \delta}{\gamma_m^{1/2}} \\ &\approx 2.92 \text{ Hz } R^{1/2} n_{\text{ISM}}^{3/4} \gamma_m^{-1/2} \eta^{1/2} \delta, \\ &\approx 5.36 \text{ Hz } R^{1/2} n_{\text{ISM}}^{3/4} \gamma_m^{-1/2} \Gamma_{\text{sh}}^{1/2} \delta. \end{aligned} \quad (34)$$

Hereafter, we use a typical value,  $s = 2.5$ , in numerical estimates.

### 3.2.2. Case $\alpha = 1$

This case may be relevant to the late afterglow from a jet.

$$\begin{aligned}\nu'_a &\simeq (s-1) \frac{\pi}{24} \frac{(R/c)\nu_{p,\text{ISM}}^2 \delta^2}{\gamma_m^3} \\ &\approx 5.28 \times 10^{-4} \text{ Hz } R n_{\text{ISM}} \gamma_m^{-3} \delta^2.\end{aligned}\quad (35)$$

### 3.3. Self-absorption frequency for $\nu_a > \nu_m$

In order to calculate the self-absorption frequency in this regime, we need the full expression for the emissivity function:

$$P(\nu', \gamma) = \frac{e^2}{2c} \delta 2\pi\nu_r J\left(\frac{\nu'}{\nu_r \gamma^2}\right), \quad (36)$$

where the function  $J(\xi)$  for  $\mu \gg 1$  and  $\delta \ll 1$  is

$$J(\xi) = (2\mu + 1)\xi^{2\mu} [I(2) - I(\xi)], \quad (37)$$

$$I(\xi) = -\left(\frac{\xi^{-2\mu+1}}{2\mu-1} - \frac{\xi^{-2\mu+2}}{2\mu-2} + \frac{1}{2} \frac{\xi^{-2\mu+3}}{2\mu-3}\right). \quad (38)$$

This function corresponds to the  $\alpha = 1$  case. The expression for the  $\alpha = 0$  is more complicated. Our analysis indicates, however, that the jitter emissivity function is approximated by a sharply broken power-law very well (much better than the synchrotron one does). Therefore, we will use the approximate expression for  $J(\xi)$ , which describes well the  $\alpha = 1$  and  $\alpha = 0$  spectra. We use

$$J(\xi) = \begin{cases} \xi^\alpha, & \text{if } \xi < 2, \\ 0, & \text{if } \xi \geq 2. \end{cases} \quad (39)$$

This function mimics a power-law spectrum up to the peak jitter frequency  $\nu_j \simeq 2\nu_r \gamma^2$ , with the sharp cutoff above it.

The opacity is:

$$\kappa_{\nu'} = \frac{(s+2)(s-1)N_e \gamma_m^{s-1}}{8\pi m_e V_{\text{bw}} \nu'^2} \frac{e^2}{2c} \delta 2\pi\nu_r \int_{\gamma_m}^{\infty} J\left(\frac{\nu'}{\nu_r \gamma^2}\right) \gamma^{-s-1} d\gamma. \quad (40)$$

Upon substitution of  $J(\xi)$  the integral becomes

$$\frac{1}{2} \left(\frac{\nu}{\nu_r}\right)^{-s/2} \int_0^{\min(\nu' / (\nu_r \gamma_m^2); 2)} z^{\alpha+s/2-1} dz. \quad (41)$$

We are interested in the high-energy part of the spectrum, above  $\nu' \gg \nu'_m \simeq 2\nu_r\gamma_m^2$ . Therefore, the upper limit in the integral is equal to 2. Thus, we have for the opacity at frequencies above the spectral peak:

$$\kappa_{\nu'} = \frac{(s+2)(s-1)}{(s+2\alpha)} \frac{2^{s/2+\alpha-3}}{12\pi} \frac{(R/c)\omega_{p,e,ISM}^2}{\Delta'\gamma_m^3} \frac{\delta^2}{\nu'_m} \left( \frac{\nu'}{\nu'_m} \right)^{-s/2-2}. \quad (42)$$

Since  $F_\nu \propto \nu^{5/2}$  for  $\nu_m < \nu < \nu_a$ , rather than  $\propto \nu^2$ , the absorption frequency should be defined as the frequency at which  $dF_\nu/d\nu = 0$ , where  $F_\nu \propto \nu^{5/2}(1 - e^{-\kappa_{\nu'}\Delta'})$ . For a simple estimate, we can still use the condition:  $\kappa_{\nu'_a}\Delta' \simeq 1$ . We have

$$\nu'_a \simeq \left( 2^{s/2+\alpha-3} \frac{\pi}{3} \frac{(s+2)(s-1)}{(s+2\alpha)} \right)^{2/(s+4)} \left[ \frac{(R/c)\nu_{p,ISM}^2 \nu_m^{s/2+1} \delta^2}{\gamma_m^3} \right]^{2/(s+4)}. \quad (43)$$

The peak frequency,  $\nu'_m$ , is calculated in the next section, Eq. (45). To proceed furter, we again use the typical value of the electron power-law exponent,  $s = 2.5$ . For such  $s$ , the values of the numerical factor (the first term) in Eq. (43) is equal to 0.95 and 0.99 for  $\alpha = 0$  and  $\alpha = 1$ , respectively. We, therefore use the representative value of 0.97 for both cases, which gives an error in the  $\nu'_a$  value to within a couple of percents. Thus,

$$\nu'_a \approx 320 \text{ Hz } R^{0.31} n_{ISM}^{0.65} \Gamma_{sh}^{0.69} \gamma_m^{0.46} \delta^{0.62}. \quad (44)$$

### 3.4. Peak frequency

The peak frequency of the shock spectrum (from an ensemble of electrons) is determined by the jitter frequency at  $\gamma_m$ :

$$\begin{aligned} \nu'_m &\simeq 2\nu_r\gamma_m^2 \\ &\approx 1.80 \times 10^4 \text{ Hz } n_{ISM}^{1/2} \gamma_m^2 \eta \\ &\approx 6.04 \times 10^4 \text{ Hz } n_{ISM}^{1/2} \Gamma_{sh} \gamma_m^2. \end{aligned} \quad (45)$$

### 3.5. Cooling break frequency

The total (integrated over frequencies) emitted power by an electron is identical in jitter and synchrotron regimes. Thus, the cooling break is unchanged. We quote results from Sari et al. (1998)

$$\nu'_c = (3/2)\nu_B\gamma_c^2, \quad (46)$$

where the cooling Lorentz factor (neglecting Compton losses) is

$$\gamma_c = \frac{3m_e}{16m_p c \sigma_T \epsilon_B} \frac{1}{n_{\text{ISM}} \Gamma_{\text{sh}} t_{\text{loc}}} \quad (47)$$

where  $t_{\text{loc}} = t/(1+z)$  is the cosmologically local time for a GRB. Thus,

$$\nu'_c \approx 4.29 \times 10^{24} \text{ Hz } n_{\text{ISM}}^{-3/2} \Gamma_{\text{sh}}^{-5} \epsilon_B^{-3/2} t_{\text{loc}}^{-2}. \quad (48)$$

## 4. Observables

The power-law segments in  $\nu_a < \nu_m$  and  $\nu_a > \nu_m$  regimes are, respectively:

$$F_{\nu}^{(\nu_a < \nu_m)} \propto \begin{cases} \nu^2, & \text{if } \nu < \nu_a; \\ \nu^{\alpha}, & \text{if } \nu_a < \nu < \nu_m; \\ \nu^{-(s-1)/2}, & \text{if } \nu_m < \nu < \nu_c; \\ \nu^{-s/2}, & \text{if } \nu_c < \nu. \end{cases} \quad (49)$$

$$F_{\nu}^{(\nu_a > \nu_m)} \propto \begin{cases} \nu^2, & \text{if } \nu < \nu_m; \\ \nu^{5/2}, & \text{if } \nu_m < \nu < \nu_a; \\ \nu^{-(s-1)/2}, & \text{if } \nu_a < \nu < \nu_c; \\ \nu^{-s/2}, & \text{if } \nu_c < \nu. \end{cases} \quad (50)$$

### 4.1. Frequencies: ISM

We now calculate the frequencies in the observer's frame (thus, all frequencies are boosted by  $\Gamma_{\text{sh}}/(1+z)$ ) and their dependencies on the burst parameters for  $s = 2.5$ .

$$\nu_a^{(\alpha=0)} \approx 5.88 \times 10^8 \text{ Hz } (1+z)^{-3/4} E_{52}^{1/4} \epsilon_e^{-1/2} \delta n_{\text{ISM},0}^{1/2} t_{\text{days}}^{-1/4}, \quad (51)$$

$$\nu_a^{(\alpha=1)} \approx 9.56 \times 10^4 \text{ Hz } (1+z)^{-2} E_{52}^0 \epsilon_e^{-3} \delta^2 n_{\text{ISM},0} t_{\text{days}}, \quad (52)$$

$$\nu_a^{(>\nu_m)} \approx 3.13 \times 10^{10} \text{ Hz } (1+z)^{-0.27} E_{52}^{0.35} \epsilon_e^{0.46} \delta^{0.62} n_{\text{ISM},0}^{0.30} t_{\text{days}}^{-0.73}, \quad (53)$$

$$\nu_m \approx 4.02 \times 10^{12} \text{ Hz } (1+z)^{1/2} E_{52}^{1/2} \epsilon_e^2 t_{\text{days}}^{-3/2}, \quad (54)$$

$$\nu_c \approx 8.54 \times 10^{16} \text{ Hz } (1+z)^{-1/2} E_{52}^{-1/2} \epsilon_{B,-3}^{-3/2} n_{\text{ISM},0}^{-1} t_{\text{days}}^{-1/2}. \quad (55)$$

Here we also quoted the result from Sari et al. (1998) for the cooling frequency in the adiabatic regime of blast wave evolution in the constant ISM density environment, corrected for the redshift.

Finally, we compute the peak flux of jitter afterglows by using the relation  $F_{\nu,\max} = \delta^2 F_{\nu,\max,\text{synch}} \nu_m / \nu_{m,\text{synch}}$  and the synchrotron peak flux from Sari et al. (1998):

$$F_{\nu,\max} = 10^3 E_{52} \epsilon_{B,-3} n_{ISM,0} D_{28}^{-2} \mu Jy \quad (56)$$

We remind that the jitter deflection parameter is related to the magnetic field equipartition parameter as follows:

$$\delta \approx 36.0 \epsilon_B^{1/2} \approx 1.12 \epsilon_{B,-3}^{1/2}. \quad (57)$$

Figure 1 shows the jitter and synchrotron spectra for an afterglow with  $E = 10^{53}$  erg,  $\epsilon_e = 0.1$ ,  $\epsilon_B = 0.0001$ ,  $n_{ISM} = 1$  and  $s = 2.5$ , computed at  $t = 0.1, 1$  and  $10$  days.

#### 4.2. Frequencies: Wind

We now calculate the frequencies in the observer's frame in the wind environment.

$$\nu_a^{(\alpha=0)} \approx 2.79 \times 10^9 \text{ Hz} (1+z)^{-1/4} E_{52}^0 \epsilon_e^{-1/2} \delta A_* t_{\text{days}}^{-3/4}, \quad (58)$$

$$\nu_a^{(\alpha=1)} \approx 1.80 \times 10^5 \text{ Hz} (1+z)^{-1} E_{52}^{-3/2} \epsilon_e^{-3} \delta^2 A_*^2 t_{\text{days}}^0, \quad (59)$$

$$\nu_a^{(>\nu_m)} \approx 1.41 \times 10^{11} \text{ Hz} (1+z)^{0.04} E_{52}^{0.58} \epsilon_e^{0.46} \delta^{0.62} A_*^{0.62} t_{\text{days}}^{-1.04}, \quad (60)$$

$$\nu_m \approx 2.40 \times 10^{13} \text{ Hz} (1+z)^{1/2} E_{52}^{3/2} \epsilon_e^2 t_{\text{days}}^{-3/2}, \quad (61)$$

$$\nu_c \approx 5.66 \times 10^{15} \text{ Hz} (1+z)^{-3/2} E_{52}^{1/2} \epsilon_{B,-3}^{3/2} A_*^{-2} t_{\text{days}}^{1/2}. \quad (62)$$

Here we also quoted the result from Chevalier & Li (2000) for the cooling frequency in the adiabatic regime of blast wave evolution in the wind environment.

#### 5. Discussion

We considered in this work the properties of GRB afterglows with radiation produced by jitter radiation instead of synchrotron. For the first time we evaluate the self absorption frequency in various regimes and for blastwaves propagating in different ambient media.

Within the present framework, we analyzed two possible regimes of the jitter mechanism. If the post-shock magnetic turbulence is isotropic (which is very likely in the far downstream region), then  $\alpha = 0$ . If the turbulence remains anisotropic throughout the shell than (i) if we observe a shock before the jet break or if the outflow is spherical, then still  $\alpha = 0$ . However, (ii) for anisotropic turbulence and late times (long after the jet break), one can have  $\alpha = 1$ .

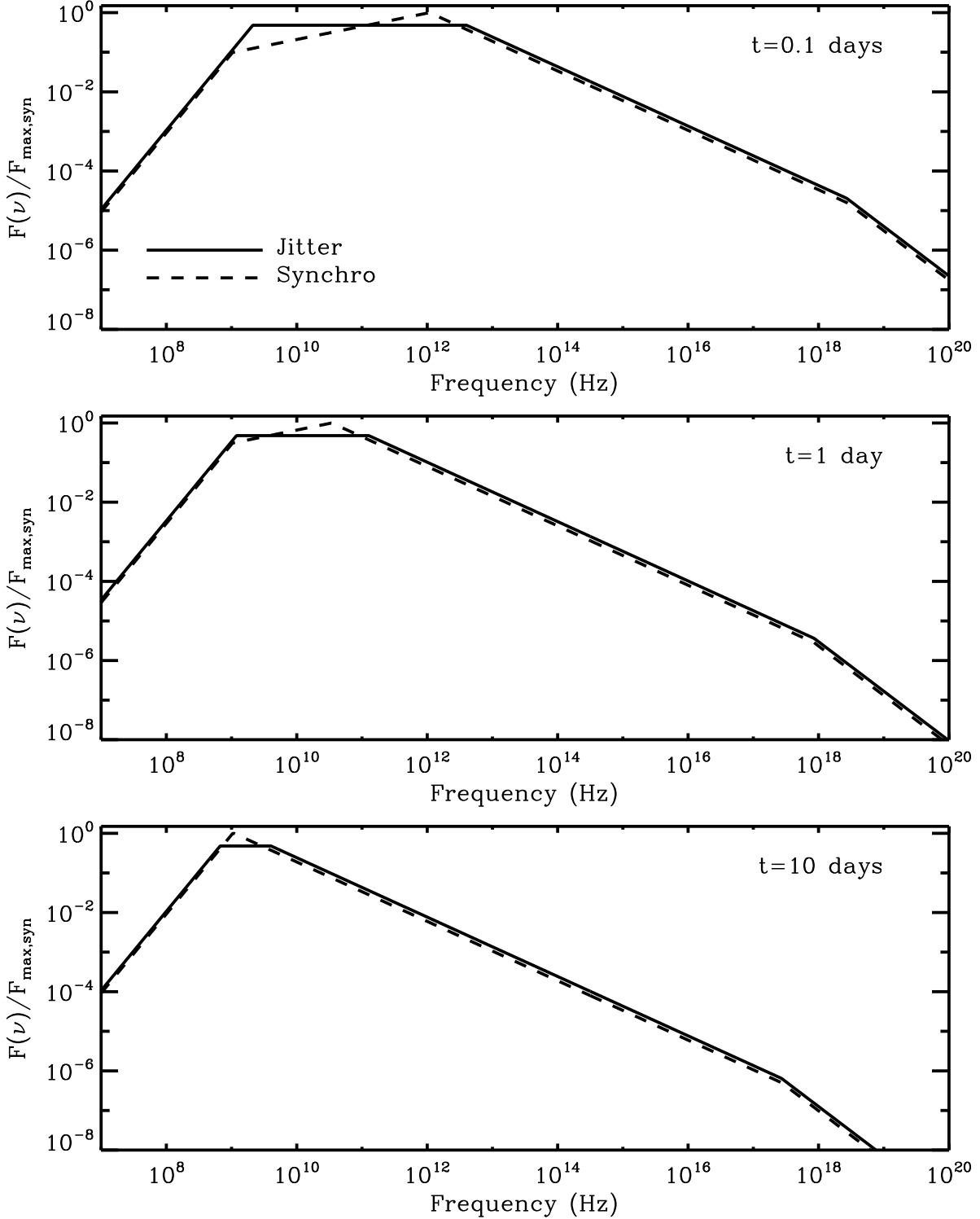


Fig. 1.— Jitter and synchrotron spectra for a typical afterglow running into a uniform medium. The parameter set is:  $E = 10^{53}$  erg,  $\epsilon_e = 0.1$ ,  $\epsilon_B = 0.0001$ ,  $n_{\text{ISM}} = 1$  and the electron energy distribution power-law index  $s = 2.5$ , computed at  $t = 0.1, 1$  and  $10$  days.

It is likely that one can have an intermediate regime for most of the time, as the properties of turbulence likely vary downstream as a function of the distance from the shock front.

Note that in the jitter regime, the peak frequency is independent of the magnetic field strength. In general, it depends on the ambient density. However, for the assumed parameter  $\eta \propto \Gamma_{\text{sh}}$ , which incorporates all details (not so well known) of the magnetic field evolution far downstream, the jitter peak is independent of the density at all, either  $n_{\text{ISM}}$  or  $A_*$ . Note also that the jitter self-absorption frequencies and the peak frequency strongly depend on the electron equipartition parameter. It may be helpful to remember that the jitter peak frequency is higher than the synchrotron peak frequency in the field of the same strength (same  $\epsilon_B$ ) and the same electron energy distribution (same  $\epsilon_e$  and the electron index  $s$ ) by a factor  $\sim \delta^{-1}$ , which, in turn, is  $\propto \epsilon_B^{1/2}$ .

Finally, we estimate the times when the emission becomes optically thick,  $\nu_a \sim \nu_m$  for both  $\alpha$ 's, for the ISM case.

$$t_a^{(\alpha=0)} \sim 1170 \text{ days} (1+z) E_{52}^{1/5} \epsilon_e^2 \delta^{-4/5} n_{\text{ISM},0}^{-2/5}, \quad (63)$$

$$t_a^{(\alpha=1)} \sim 1120 \text{ days} (1+z) E_{52}^{1/5} \epsilon_e^2 \delta^{-4/5} n_{\text{ISM},0}^{-2/5}, \quad (64)$$

$$t_a^{(\nu_m < \nu_a)} \sim 548 \text{ days} (1+z) E_{52}^{0.20} \epsilon_e^{2.00} \delta^{-0.80} n_{\text{ISM},0}^{0.40} \quad (65)$$

Ideally, these times should coincide. The discrepancies are due to the approximations made in our analysis. In particular, the self-absorption frequency for  $\nu_m < \nu_a$  is overestimated by a factor of two (as is explained above), hence the thin-to-thick transition time is earlier. A more detailed treatment of the self-absorption frequencies will be presented elsewhere (Jared et al. in preparation; Morsony et al. in preparation). Also, the time when the cooling break is equal to the peak,  $\nu_c \sim \nu_c$  is

$$t_c \sim 4.71 \times 10^{-5} \text{ days} (1+z) E_{52} \epsilon_e^2 \epsilon_{B,-3}^{3/2} n_{\text{ISM},0}. \quad (66)$$

The numerical factor in the above equation is equal to 4.07 seconds.

Similarly, we calculate  $t_a$ 's and  $t_c$  for the wind case.

$$t_a^{(\alpha=0)} \sim 1.76 \times 10^5 \text{ days} (1+z) E_{52}^2 \epsilon_e^{10/3} \delta^{-4/3} A_*^{-4/3}, \quad (67)$$

$$t_a^{(\alpha=1)} \sim 2.61 \times 10^5 \text{ days} (1+z) E_{52}^2 \epsilon_e^{10/3} \delta^{-4/3} A_*^{-4/3}, \quad (68)$$

$$t_a^{(\nu_m < \nu_a)} \sim 7.08 \times 10^4 \text{ days} (1+z) E_{52}^{2.00} \epsilon_e^{-3.35} \delta^{-1.34} A_*^{-1.34}, \quad (69)$$

$$t_c \sim 6.51 \times 10^{-2} \text{ days} (1+z) E_{52}^{1/2} \epsilon_e \epsilon_{B,-3}^{-3/4} A_*. \quad (70)$$

The discrepancies in  $t_a$ 's are, again, due to the approximations made in calculating  $\nu_a$ .

Figure 1 allows us to comment on the differences between synchrotron and jitter afterglows. The high energy part of the spectrum (mainly the optical and X-ray regimes) are

hardly distinguishable between the two mechanisms, especially if, as expected from simulation, jitter fields are created such that  $\delta \lesssim 1$ .

The two main differences are in the low energy branches, around when most radio observations are performed. First, the spectral slope at the left of the peak frequency is flat,  $\propto \nu^0$ , rather than the canonical  $\nu^{1/3}$ ; second, the location of the self-absorption break is different and evolves in time differently than in synchrotron afterglows. Since one important observation to nail down the density of the ambient medium is the radio regime, modelling afterglows with jitter radiation may lead to different results compared to those of synchrotron modelling (Morsony et al. and Workman et al., in preparation).

MM gratefully acknowledges support from the Institute for Advanced Study. This work was supported by NASA grants NNG-04GM41G (MM) and NNG-06GI06G (BM, DL), Swift Guest Investigator grant 06-SWIFT306-0001 (MM) and NNX06AB69G (BM, DL), DoE grant DE-FG02-04ER54790 (MM), and NSF grant AST-0307502 (BM, DL).

## REFERENCES

Chevalier, R. A., & Li, Z.-Y. 2000, *ApJ*, 536, 195

Dermer, C. D., & Böttcher, M., & Chiang, J. 2000, *ApJ*, 537, 225

Fleishman, G. 2006, *ApJ*, 638, 348

Frederiksen, J. T., Hededal, C. B., Haugbølle, T., Nordlund, Å. 2004 *ApJ*, 608, L13

Granot, J., Piran, T., & Sari, R. 1999, *ApJ*, 527, 236

Meszaros, P., & Rees, M. J. 1997, *ApJ*, 476, 232

Medvedev, M. V., & Loeb, A. 1999, *ApJ*, 526, 697

Medvedev, M. V. 2000, *ApJ*, 540, 704

Medvedev, M. V. 2006a, *ApJ*, 637, 869

Medvedev, M. V. 2006b, *ApJ*, 651, L9

Medvedev, M. V., Fiore, M., Fonseca, R. A., Silva, L O., Mori, W. B. 2005, *ApJ*, 618, L75

Medvedev, M. V., Silva, L. O., & Kamionkowski, M. 2006, *ApJ*, 642, L1

Nishikawa, K.-I., Hardee, P., Richardson, G., Preece, R., Sol, H., & Fishman, G. J. 2003, *ApJ*, 595, 555

Panaitescu, A. 2006, *MNRAS*, 366, 1357

Panaitescu, A., & Kumar, P. 2001, *ApJ*, 560, L49

Piran, T. 1999, *Phys. Rep.*, 314, 575

Sari, R., Piran, T., & Narayan, R. 1998, *ApJ*, 497, L17

Silva, L. O., Fonseca, R. A., Tonge, J. W., Dawson, J. M., Mori, W. B., & Medvedev, M. V. 2003, *ApJ*, 596, L121

Spitkovsky, A. 2005, in *AIP Conf. Proc. 801, Astrophysical Sources of High Energy Particles and Radiation*, ed. T. Bulik & B. Rudak (Melville: AIP), 345

Waxman, E. 1997, *ApJ*, 491, L19